

Spectropolarimetric monitoring of active galaxy 3C 390.3 with 6-m telescope SAO RAS in the period 2009–2014

V. L. Afanasiev,¹ A. I. Shapovalova,¹ L. Č. Popović^{2,3,4★} and N. V. Borisov¹

¹Special Astrophysical Observatory of the Russian Nizhnij Arkhyz, Karachaev-Cherkesia 369167, Russia

²Astronomical Observatory, Volgina 7, 11060 Belgrade 74, Serbia

³Department of Astronomy, Faculty of Mathematics, University of Belgrade, Studentski trg 16, 11000 Belgrade, Serbia

⁴Isaac Newton Institute of Chile, Yugoslavia Branch, Belgrade, Serbia

Accepted 2015 January 28. Received 2015 January 27; in original form 2014 August 23

ABSTRACT

Here we present the spectropolarimetric observations of the radio-loud active galaxy 3C 390.3 in the period 2009–2014 (24 epochs). The galaxy has been observed with the 6-m telescope of Special Astrophysical Observatory of the Russian Academy of Science (SAO RAS) using the Spectral Camera with Optical Reducer for Photometric and Interferometric Observations (SCORPIO) spectropolarimeter. We explore the variability and lags in the polarized light of the continuum and broad H α line. We give the Stokes parameters Q , U , degree of linear polarization P and the position angle of the polarization plane, φ , for 24 epochs.

We find a small lag (10–40 d) between the unpolarized and polarized continuum that is significantly smaller than the estimated lags for the unpolarized broad emission lines (lag(H α) \sim 138–186 and lag(H β) \sim 60–79 d). This shows that the region of the variable polarized continuum is significantly smaller than the broad line region, indicating that a part of the polarized continuum is coming from the jet. The lag of the polarized light in the H α line (89–156 d) indicates an additional component to the disc one that has an outflowing velocity of \sim 1200 km s⁻¹. This region seems to depolarize the polarized broad H α line emitted from the disc and scattered in the inner part of the torus.

Key words: line: profiles – galaxies: active – quasars: individual: 3C 390.3.

1 INTRODUCTION

The radio-loud active galactic nucleus (AGN) 3C 390.3 ($z = 0.0561$) belongs to a group of 10 per cent AGN with double-peaked broad Balmer lines. It is well known that 3C 390.3 shows a strong variability (to \sim 5 times) in the ultraviolet (UV)/optical continuum and broad lines (see Barr et al. 1980; Yee & Oke 1981; Netzer 1982; Barr, Willis & Wilson 1983; Penston & Perez 1984; Clavel & Wamsteker 1987; Veilleux & Zheng 1991; Zheng 1996; Wamsteker et al. 1997; Dietrich et al. 1998, 2012; O’Brien et al. 1998; Shapovalova et al. 2001, 2010; Sergeev et al. 2002; Tao et al. 2008; Gupta, Srivastava & Wiita 2009; Popović et al. 2011). Furthermore, 3C 390.3 has a high variability in the X-ray spectrum, where a broad Fe K α line is present (Inda et al. 1994; Eracleous, Halpern & Livio 1996; Leighly & O’Brien 1997; Wozniak et al. 1998). The X-ray emission varies in a scale of several days, showing the highest variability in the lower energy region (Gliozzi, Sambruna & Eracleous 2003; Gupta et al. 2009), while the UV/optical broad lines vary at scales of several tens to hundred light days (see e.g. Clavel & Wamsteker 1987;

Wamsteker et al. 1997; Dietrich et al. 1998, 2012; O’Brien et al. 1998; Shapovalova et al. 2001, 2010; Sergeev et al. 2002).

Although the broad double-peaked emission lines of 3C 390.3 are probably emitted from an accretion disc, there are some questions about the nature of the broad line region (BLR), as e.g. Zheng, Veilleux & Grandi (1991) argued that a radial biconical outflow is present in the BLR, but cross-correlation function (CCF) analysis shows that there is no delay between the blue and red wings of H β , that indicates a dominant circular motion in the BLR (Dietrich et al. 1998, 2012; Shapovalova et al. 2001, 2010; Zheng 2011, 2013). However, besides two peaks from the disc, there is an additional central, slightly redshifted, component in the profiles of the broad lines (Shapovalova et al. 2010; Popović et al. 2011). Also, from time to time, there are some kind of perturbations in the disc (Jovanović et al. 2010; Popović et al. 2011). Moreover, from a detailed study of the profiles of the H α and H β broad emission lines in the monitored period (1995–2007), Popović et al. (2011) have shown that the geometry of the BLR of 3C 390.3 seems to be very complex but the BLR with the disc-like geometry has a dominant emission. On the contrary, spectropolarimetric observations (Corbett et al. 1998, 2000) indicate a BLR model in which the H α emission line is formed in the biconical flow and the polarized

* E-mail: lpopovic@aob.rs

component of the line is scattered on the inner part of the torus. The possible jet influence on the BLR and continuum emission has been discussed in Arshakian et al. (2008, 2010). They found an observational evidence for the connection between the variable optical continuum of 3C 390.3 nucleus, the compact radio emission of the jet on the sub-parsec scale and emissions of new observed jet components. To explain these correlations, they suggested that the variable optical continuum emission originates in the innermost part of the jet.

Note here that the double-peaked broad line profiles, in this and other double-peaked AGN, could be explained with a number of different models for the BLR, as e.g. supermassive binary black holes (Gaskell 1983, 1996; Popović 2012), outflowing biconical gas streams (Zheng et al. 1991), in the accretion disc (Perez et al. 1988; Rokaki, Boisson & Collin-Souffrin 1992), two-arm spiral waves in the accretion disc (Chakrabarti & Wiita 1994) or a relativistic eccentric (elliptic) disc (Eracleous et al. 1995), etc.

We performed the spectropolarimetric observations of 3C 390.3 with 6-m telescope of Special Astrophysical Observatory of the Russian Academy of Science (SAO RAS) in the period 2009–2014 period with the aim to explore the disagreement between optical monitoring results which indicate dominant disc-like emission (see e.g. Dietrich et al. 1998, 2012; Shapovalova et al. 2001, 2010; Jovanović et al. 2010; Popović et al. 2011; Zheng 2011, 2013, and reference therein) and spectropolarimetric observations which are in favour of the biconical flow in the BLR (Corbett et al. 1998, 2000). Here we present the analysis of spectropolarimetric observations of 3C 390.3 obtained in 24 epochs and study how the parameters of the linear polarization change with time in the broad H α emission line and continuum.

The paper is organized as following: in Section 2 we describe our observations and data reduction; in Section 3 the results are given; in Section 4 we discuss obtained results and finally in Section 5 we outline conclusions.

2 OBSERVATIONS AND DATA REDUCTION

2.1 Observation

In the period 2009–2014 we performed spectropolarimetric monitoring of the broad line radio galaxy 3C 390.3 (24 epochs) with the 6-m telescope of SAO RAS using the modified spectrograph Spectral Camera with Optical Reducer for Photometric and Interferometric Observations (SCORPIO; Afanasiev & Moiseev 2005, 2011) in the mode of the spectropolarimetry and polarimetry in the spectral range 4000–8000 Å with the spectral resolution 4–10 Å. We used two types of polarization analysers: the single Wollaston prism (WOLL-1) separates the ordinary and extraordinary rays in two planes 0° and 90° and a double Wollaston prism (WOLL-2) consisting of two prisms illuminating half of the parallel beam and polarized light is separating planes in 0°, 90°, 45° and 135°. For an unambiguous measurement of parameters of the linear polarization in the first case it is required to obtain a sequence of four pairs of spectra at different angles of the phase plate (0:45, 22:5 and 67:5), with WOLL-1 registering two long-slit spectra (with a slit 1–2 arcsec width and 120 arcsec height). The second case records simultaneously four long-slit spectra (60 arcsec height) that uniquely define the parameters of the linearly polarized radiation. For calibration purposes, each night we observed the polarization of standard stars from the list of Hsu & Breger (1982) and Schmidt, Elston & Lupie (1992). Additionally, we observed non-polarized stars as spectrophotometric standards. We found that the accu-

racy of the linear polarization measurements is ~ 0.1 per cent (more details in Afanasiev & Moiseev 2005; Afanasiev & Amirkhanyan 2012; Afanasiev et al. 2014a). The typical differences between our measurements of polarization standards and those in the catalogue were 0.1–0.2 per cent for polarization and 2°–4° for the polarization angle.

In Table 1 the log of observations is given, where following are listed: Julian date, total exposure time, number of polarization cycles, seeing, slit, analyser, grating and spectral resolution. We observed in three different modes, using gratings VPHG550G, VPHG940 and VPHG1200 which covered the H β and H α wavelength ranges. Additionally we observed the interstellar matter (ISM) polarization with the filter V at $\lambda(\text{max})$ 5500 Å. The number of cycles denotes a number of observations for each position angle in the phase plate, i.e. one cycle corresponds to the observations in all four above-mentioned angles. The spectral resolutions given in Table 1 were estimated using the full width at half-maximum (FWHM) of the lines from the night sky in the integral (AGN+night sky) spectra.

From Table 1 it can be seen that there were large seeing variations between observations during the monitoring period. This may cause changes in polarization because the relative contribution of unpolarized host galaxy light will change with the seeing, however, for this galaxy it is not a major problem, since the emission of the nucleus is very bright compared to the host galaxy.

2.1.1 Polarization of the ISM

The observed linear polarization of an object is a vector composition of the ISM polarization (\mathbf{P}_{ISM}) and polarization of the object (\mathbf{P}_{AGN} – in this case the radio galaxy 3C 390.3), i.e. $\mathbf{P}_{\text{obs}} = \mathbf{P}_{\text{AGN}} + \mathbf{P}_{\text{ISM}}$. The ISM polarization, as it is well known, depends on the Galactic latitude and it has strong changes in the rate of polarization and in the polarization angle on 1° scale on celestial sphere. That is connected with non-homogeneous distribution of the ISM. In a number of papers, the ISM polarization has been taken into account as a function of the Galactic extinction $E(B - V)$ for different latitudes as it is described in Serkowski, Mthewson & Ford (1975). However, the problem with this method is that it does not take into account the direction of the ISM polarization vector, i.e. the vector \mathbf{P}_{ISM} has direction and intensity and both quantities should be taken into account (see e.g. Kishimoto et al. 2004). Therefore, here we take into account the ISM polarization vector by measuring polarization of a number of stars around the AGN, which represents the ISM polarization. For these observations we used the wide-field polarimetry, as within the range of 0.45–0.8 mkm a typical change in the ISM polarization is smaller than 10 per cent from the maximum, i.e. for Galactic longitudes $> 25^\circ$ the estimate of wide-field \mathbf{P}_{ISM} is satisfactory for this purposes.

For the ISM polarization estimation we used WOLL-1 analyser with rotated $\lambda/2$ phase plate, and with the 3–5 arcmin field. We considered only bright surrounding stars within 3 arcmin around 3C 390.3 in the V filter. We found 11 brightest stars in the field and for each star we calculated parameters Q and U .¹ We calculated for each of star parameters Q and U and estimated the averaged polarization parameters of the ISM to be $Q_{\text{ISM}} = 0.64 \pm 0.23$ per cent, $U_{\text{ISM}} = -0.51 \pm 0.20$ per cent, $P_{\text{ISM}} = 0.82 \pm 0.22$ per cent and

¹ For more detailed procedure of polarization parameters calculation in the image mode see Afanasiev, Rosenbush & Kiselev (2014b).

Table 1. Log of observations.

Date observation	JD 240 000+	Total exposure (s)	Num. of cycles	Seeing (arcsec)	Slit (arcsec)	Analyser	Grating/ filter	Spectral resolution (Å)
2009.09.24	55099	3600	6	1	2.5	WOLL-1	VPHG550G	20
2010.07.17	55394	2400	5	2	2	WOLL-1	VPHG940	7
2010.11.01	55501	3600	5	1.5	1	WOLL-1	VPHG940	5
2011.05.01	55682	2160	3	2.5	2	WOLL-1	VPHG1200	6
2011.06.01	55713	4000	5	1.6	1.5	WOLL-1	VPHG940	6
2011.08.26	55799	1320	11	2.5	2	WOLL-2	VPHG940	6
2011.09.27	55831	2400	5	1.6	2	WOLL-1	VPHG1200	5
2011.11.20	55885	2880	6	2.5	1	WOLL-1	VPHG940	4
2012.02.01	55959	1440	3	4	1	WOLL-1	VPHG940	4
2012.02.14	55971	4320	6	3	2	WOLL-1	VPHG940	6
2012.04.15	56032	2880	6	3	2	WOLL-1	VPHG940	6
2012.05.17	56064	2400	5	1.2	2	WOLL-1	VPHG1200	5
2012.06.21	56099	2880	6	1.3	2	WOLL-1	VPHG1200	5
2012.06.21	56099	600	15	1.5	Image	WOLL-1	Jonson V	–
2012.08.24	56163	2160	6	1.2	2	WOLL-1	VPHG940	6
2012.09.11	56181	2400	8	2.5	2	WOLL-1	VPHG940	5
2012.10.07	56207	3600	8	2	2	WOLL-1	VPHG940	6
2012.11.13	56244	2400	5	1	2	WOLL-1	VPHG940	7
2013.02.06	56329	2400	8	3	2	WOLL-1	VPHG940	6
2013.06.15	56458	4800	8	1	2	WOLL-1	VPHG940	6
2013.11.03	56599	1260	21	3	2	WOLL-2	VPHG940	6
2014.02.25	56713	3480	29	2	1	WOLL-2	VPHG940	4
2014.03.06	56722	3600	20	2	2	WOLL-2	VPHG940	6
2014.03.25	56741	3600	30	1.5	2	WOLL-2	VPHG940	5
2014.05.30	56807	3600	30	2	1	WOLL-2	VPHG940	4

$\varphi_{\text{ISM}} = 160.7 \pm 6.2$. Further in the text we will use the polarization parameters corrected for the ISM polarization.

Note here that in the catalogue of Heiles (2000) the rate of ISM polarization is changing around 0.5–1.1 per cent and angle of ISM polarization around 159° – 163° in the radius of 5° , that is not in contradiction with our estimates.

The contribution of the interstellar polarization (ISP) of the host galaxy of 3C 390.3 has not been considered, since, as it is mentioned above, the nucleus is significantly brighter than the host galaxy, and there is a problem to find the host galaxy ISP even using the [O III] lines, because in that case one assumes that these lines are intrinsically unpolarized, which may not be the case.

2.2 Data reduction

The data reduction includes standard procedure for the long-slit spectroscopy, bias, flat-field, geometrical correction along the slit, correction of the spectral line curvature, night sky subtraction, spectral sensitivity of the instrument and spectral wavelength calibration. Additionally we used a comparison star in order to remove the strong atmospheric bands of O2 – $B(6870 \text{ \AA})$ and $A(7600 \text{ \AA})$ from 3C 390.3 spectrum. Note that the B band is on the blue wing of H α . We integrated spectra along the slit, since the procedure of decomposition (of the observed light as a function of wavelength along the slit) of the host galaxy and AGN increases the statistical errors. Integration interval was $\pm(10$ – $15 \text{ arcsec})$. This systematic error due to wings image does not exceed 0.1 per cent in the value of the degree of polarization.

Values of normalized Stokes parameters $Q(\lambda)$, $U(\lambda)$ and total intensity $I(\lambda)$ for WOLL-1 analyser can be found from the simple relations (see also Afanasiev et al. 2014a):

$$Q(\lambda) = \frac{1}{2} \left(\frac{I_0(\lambda) - I_{90}(\lambda)}{I_0(\lambda) + I_{90}(\lambda)} \right)_{\phi=0} - \frac{1}{2} \left(\frac{I_0(\lambda) - I_{90}(\lambda)}{I_0(\lambda) + I_{90}(\lambda)} \right)_{\phi=22.5},$$

$$U(\lambda) = \frac{1}{2} \left(\frac{I_0(\lambda) - I_{90}(\lambda)}{I_0(\lambda) + I_{90}(\lambda)} \right)_{\phi=0} - \frac{1}{2} \left(\frac{I_0(\lambda) - I_{90}(\lambda)}{I_0(\lambda) + I_{90}(\lambda)} \right)_{\phi=67.5},$$

$$I(\lambda) = \sum_{\phi} [I_0(\lambda) + I_{90}(\lambda)]_{\phi}, \quad \phi = 0, 45, 22.5, 67.5.$$

For WOLL-2 analyser appropriate values are determined from the relations:

$$Q(\lambda) = \frac{I_0(\lambda) - I_{90}(\lambda)}{I_0(\lambda) + I_{90}(\lambda)},$$

$$U(\lambda) = \frac{I_{45}(\lambda) - I_{135}(\lambda)}{I_{45}(\lambda) + I_{135}(\lambda)},$$

$$I(\lambda) = I_0(\lambda) + I_{90}(\lambda) + I_{45}(\lambda) + I_{135}(\lambda).$$

Then we calculated the degree of the linear polarization $P(\lambda)$ and angle of polarization plane $\varphi(\lambda)$ as

$$P(\lambda) = \sqrt{Q(\lambda)^2 + U(\lambda)^2}, \quad \varphi(\lambda) = \frac{1}{2} \arctg[U(\lambda)/Q(\lambda)].$$

Using the procedure of the polarization parameter calculation from Afanasiev & Amirkhanyan (2012) we estimated the Stokes parameters ($I(\lambda)$, $Q(\lambda)$ and $U(\lambda)$), the degree of the linear polarization $P(\lambda)$ and position angle of polarization plane $\varphi(\lambda)$ for the rest wavelength 5500 \AA . Also we determined the continuum flux and the shift of the broad emission line in the polarized light relatively to the systematic velocity $\Delta V = V_{\text{pol}} - V_{\text{sys}}$. In further analysis, the polarization parameters (I , Q , U , P and φ) have been robustly estimated as average

in a spectral window of 25–30 Å for all cycles of measurements, the number of the windows for different observation data is between 5 and 10.

We measured the continuum flux at rest wavelength 5100 Å taking an averaged continuum in the H β wavelength range. To measure an averaged flux of the polarized continuum, we used a window of the half-width of 500 Å. To avoid the contribution of the [O III] 4959, 5007 Å lines we centred the window at 5500 Å.

Fig. 1 shows a typical observed spectrum of the unpolarized and polarized flux and its polarization parameters of 3C 390.3 obtained on 2014 May 30 in the instrumental unit without the flux calibration. As it can be seen in Fig. 1 there practically is no difference between the polarized continuum measured at rest 5100 and 5500 Å, i.e. the difference is within the error bars.

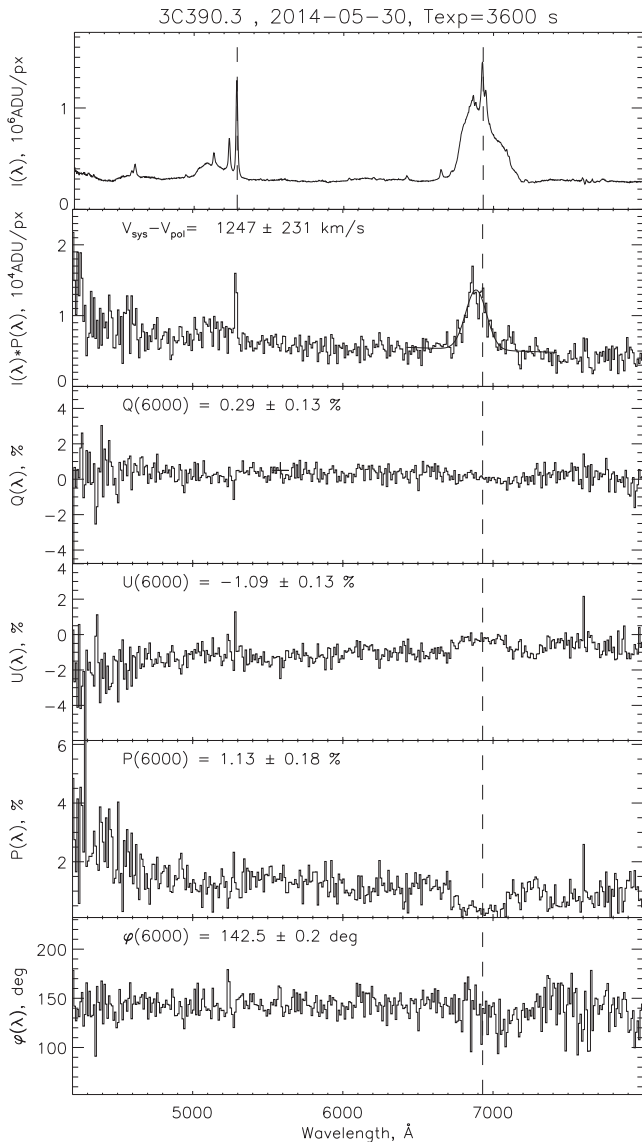


Figure 1. The observed spectrum of the unpolarized and polarized flux and its polarization parameters of 3C 390.3 on 2014 May 30. From top to bottom: the observed spectrum $I(\lambda)$, the polarized spectrum $I(\lambda)P(\lambda)$, normalized Stokes parameters $Q(\lambda)$ and $U(\lambda)$, degree of linear polarization $P(\lambda)$ and angle of the polarization plane $\varphi(\lambda)$. Spectra have been corrected for the spectral sensitivity and ISM polarization. The atmospheric absorption is removed.

From the observed H α and H β lines we removed (using Gauss decomposition) the narrow forbidden lines and obtained the broad components. Then we subtracted the continuum and obtained the broad emission line fluxes. For the absolute flux calibration we used the fluxes of the [O III] 4959 + 5007 Å – forbidden lines, taking the fluxes from Veilleux & Zheng (1991) (flux([O III]) = 1.7×10^{-13} erg cm $^{-2}$ s $^{-1}$). Sergeev et al. (2002) found that for mean seeing of 2.5 arcsec, the stellar contribution to continuum in the H α region for aperture 2×11 arcsec 2 is 7.0×10^{-16} erg cm $^{-2}$ s $^{-1}$ Å $^{-1}$. We estimated that the mean continuum flux at the rest wavelength of 5100 Å for the similar aperture is $F(\text{cnt}) \sim (3.02 \pm 0.63) \times 10^{-15}$ erg cm $^{-2}$ s $^{-1}$ Å $^{-1}$. Thus the contribution of the stellar radiation (host galaxy) to the continuum of the AGN 3C 390.3 is ~ 20 per cent. We estimated that this contribution of the host galaxy is depolarizing the AGN continuum radiation less than <0.25 per cent.

3 RESULTS

Observed polarization parameters in the continuum and broad H α line are given in Table 2, where we give the unpolarized (at 5100 Å) and polarized continuum (at 5500 Å) flux, the polarization parameters corrected for the ISM polarization, the broad H β and H α line fluxes, the polarized H α flux and the difference between the systematic and polarized line velocity ($V_{\text{sys}} - V_{\text{pol}}$) for the broad H α line. Note here that, due to large error bars in the H β wavelength range, we did not measure the polarization parameters for H β .

In Fig. 1 we show spectrum observed on 2014 May 30. The slight changes can be noticed in the rest 23 epochs, but some characteristic structures are the same in all spectra. From Fig. 1 and Table 2, one can see several characteristics in unpolarized and polarized spectra of 3C 390.3:

(i) in the unpolarized 3C 390.3 spectrum the double-peaked broad emission lines of H α and H β are present; the blue peak was always brighter than the red one during the monitored period, while the polarized component is single peaked;

(ii) the degree of the linear polarization in the continuum was always somewhat higher ~ 2 per cent in the shorter wavelengths (4000 Å), changing to ~ 1.5 per cent at 8000 Å, i.e. there is a trend to increase the linear polarization with decreasing wavelength (i.e. $P \sim 1/\lambda$);

(iii) in the polarized light we observed the H α (sometimes H β) broad emission line, shifted to the blue at $\Delta V = V_{\text{pol}} - V_{\text{sys}} = -1247 \pm 231$ km s $^{-1}$ with respect to the systematic velocity;

(iv) in the H α line the linear polarization P is always less than ~ 0.2 per cent and has a box-like shape, i.e. $P(\text{H}\alpha)$ has no pronounced structural features (there are no double peaks).

3.1 Variability in the continuum and broad H α polarization

The polarization in the continuum has a slight dependence on wavelength and varied between 1 and 2 per cent (see Fig. 2). In Fig. 2 we present the variability in the continuum at 5100 Å and polarized continuum measured at 5500 Å. As it can be seen in Fig. 2 and Table 2, the variations in the linear polarization P per cent sometimes anticorrelate with the continuum flux, i.e. the minimum value of the continuum flux corresponds to the maximum value of the linear polarization (e.g. in the period 26.08.2011–13.11.2012 or JD 245 5799–JD 245 6244). The angle of the polarization plane of the continuum reaches maximum values ($\sim 180^\circ$) in the period

Table 2. Observed Stokes parameters Q and U of the continuum, degree of polarization and polarization angle, fluxes in continuum, broad lines $H\beta$ and $H\alpha$, polarized broad $H\alpha$ and its shift. The polarized spectra have been corrected on the ISM polarization.

JD 240 000+	$Q(5500)$ (per cent)	$U(5500)$ (per cent)	$P(5500)$ (per cent)	$\varphi(5500)$ ($^\circ$)	Flux continuum 5100 \AA	Flux broad $H\beta$	Flux broad $H\alpha$	Flux polarized $H\alpha$	$V_{\text{pol}} - V_{\text{sys}}$ (km s^{-1})
55098	-0.04 ± 0.24	-1.19 ± 0.28	1.19 ± 0.24	134.0 ± 1.7	4.49 ± 0.03	3.74 ± 0.24	2.12 ± 0.26	2.37 ± 0.16	-800 ± 300
55394	-0.27 ± 0.32	-1.35 ± 0.40	1.38 ± 0.06	129.4 ± 5.0	1.97 ± 0.05	3.11 ± 0.20	1.26 ± 0.18	1.08 ± 0.32	-1559 ± 441
55501	1.30 ± 0.28	-0.10 ± 0.24	1.30 ± 0.35	177.9 ± 9.0	2.46 ± 0.12	2.93 ± 0.43	1.54 ± 0.26	2.11 ± 0.87	-1250 ± 765
55682	0.85 ± 0.11	-0.15 ± 0.10	0.86 ± 0.11	175.0 ± 2.0	4.13 ± 0.05	3.61 ± 0.18	1.41 ± 0.18	1.21 ± 0.27	-1416 ± 452
55713	1.06 ± 0.14	0.50 ± 0.14	1.18 ± 0.14	192.7 ± 2.3	4.19 ± 0.07	3.86 ± 0.34	2.27 ± 0.27	4.02 ± 0.40	-1294 ± 402
55799	0.33 ± 0.17	-1.63 ± 0.18	1.66 ± 0.05	140.8 ± 0.6	2.76 ± 0.06	4.06 ± 0.23	2.82 ± 0.30	7.19 ± 0.75	-1017 ± 182
55831	0.52 ± 0.16	-1.50 ± 0.14	1.58 ± 0.19	144.5 ± 1.7	2.43 ± 0.07	3.90 ± 0.24	3.21 ± 0.55	3.40 ± 0.39	-1053 ± 238
55885	-0.12 ± 0.23	-1.57 ± 0.28	1.57 ± 0.27	132.9 ± 9.3	2.68 ± 0.12	3.56 ± 0.46	2.84 ± 0.30	2.92 ± 1.10	-1273 ± 630
55959	-0.72 ± 0.08	-1.53 ± 0.51	1.69 ± 0.49	122.5 ± 5.4	3.33 ± 0.20	4.03 ± 0.47	1.98 ± 0.29	1.49 ± 1.33	-1221 ± 362
55971	1.13 ± 0.30	-1.02 ± 0.29	1.52 ± 0.19	158.9 ± 3.5	3.25 ± 0.12	3.40 ± 0.41	2.40 ± 0.28	2.05 ± 0.92	-1144 ± 473
56032	-0.15 ± 0.20	-1.49 ± 0.17	1.50 ± 0.18	132.0 ± 2.3	2.76 ± 0.05	3.62 ± 0.23	1.44 ± 0.18	1.44 ± 0.26	-993 ± 265
56064	0.74 ± 0.19	-0.83 ± 0.13	1.11 ± 0.15	155.8 ± 2.2	3.05 ± 0.06	3.25 ± 0.29	1.15 ± 0.70	1.20 ± 0.13	-1323 ± 237
56099	-0.08 ± 0.12	-0.94 ± 0.13	0.94 ± 0.12	132.6 ± 1.9	3.61 ± 0.05	3.76 ± 0.29	1.80 ± 0.27	1.49 ± 0.17	-1014 ± 227
56163	0.10 ± 0.09	-1.20 ± 0.20	1.20 ± 0.19	137.4 ± 1.9	3.46 ± 0.04	3.86 ± 0.31	2.17 ± 0.31	1.65 ± 0.35	-1561 ± 342
56181	0.42 ± 0.15	-1.02 ± 0.13	1.10 ± 0.16	146.3 ± 2.0	3.62 ± 0.05	3.67 ± 0.26	1.87 ± 0.26	1.46 ± 0.26	-1585 ± 272
56207	0.90 ± 0.16	-1.12 ± 0.10	1.44 ± 0.14	154.4 ± 0.9	3.41 ± 0.09	4.15 ± 0.31	1.36 ± 0.18	1.75 ± 0.25	-1540 ± 231
56244	1.02 ± 0.18	-1.33 ± 0.15	1.68 ± 0.18	153.8 ± 2.0	2.80 ± 0.05	3.83 ± 0.28	1.60 ± 0.22	1.96 ± 0.30	-1238 ± 254
56329	0.15 ± 0.20	-1.17 ± 0.20	1.18 ± 0.27	138.7 ± 2.6	2.94 ± 0.10	3.57 ± 0.34	1.30 ± 0.21	1.27 ± 0.23	-1644 ± 284
56458	1.13 ± 0.15	0.01 ± 0.20	1.13 ± 0.17	180.4 ± 2.5	2.53 ± 0.06	3.42 ± 0.24	1.08 ± 0.11	0.97 ± 0.18	-1148 ± 287
56599	0.21 ± 0.14	-1.17 ± 0.14	1.19 ± 0.06	140.0 ± 2.1	2.55 ± 0.06	3.42 ± 0.30	1.03 ± 0.13	1.33 ± 0.19	-1453 ± 183
56713	0.54 ± 0.04	-1.39 ± 0.04	1.49 ± 0.10	145.6 ± 1.1	2.53 ± 0.12	3.30 ± 0.44	1.46 ± 0.21	1.08 ± 0.35	-1474 ± 431
56722	0.13 ± 0.05	-1.24 ± 0.17	1.25 ± 0.19	138.1 ± 2.8	2.45 ± 0.06	3.29 ± 0.30	1.42 ± 0.18	1.61 ± 0.27	-1312 ± 207
56741	0.13 ± 0.05	-0.97 ± 0.11	0.98 ± 0.14	138.8 ± 0.5	2.51 ± 0.06	3.29 ± 0.32	1.44 ± 0.19	1.02 ± 0.26	-999 ± 372
56807	0.29 ± 0.13	-1.09 ± 0.13	1.13 ± 0.18	142.5 ± 0.2	2.83 ± 0.05	3.45 ± 0.27	1.48 ± 0.16	1.03 ± 0.21	-1247 ± 231

Notes. Units: continuum 5100 \AA in $10^{-15} \text{ erg cm}^{-2} \text{ s}^{-1} \text{ \AA}^{-1}$; broad $H\beta$ in $10^{-13} \text{ erg cm}^{-2} \text{ s}^{-1}$; broad $H\alpha$ in $10^{-12} \text{ erg cm}^{-2} \text{ s}^{-1}$; polarized $H\alpha$ in $10^{-14} \text{ erg cm}^{-2} \text{ s}^{-1}$.

01.11.2010–01.06.2011 or JD 245 5501–JD 245 5713. The shift of the polarized broad $H\alpha$ line had no significant change during the monitored period (almost within the error bars).

In Fig. 3 the light curves for the total and polarized continuum flux at 5100 \AA are shown.² A fast inspection of the light curves of the unpolarized and polarized continuum shows that they are in correlation.

The variation in the polarized continuum as well as the variation in the broad $H\alpha$, $H\beta$ lines, and polarized $H\alpha$ line follows the variation in the unpolarized one, but with some lags between them (Fig. 3).

In Table 3 we defined several parameters characterizing the variability of the polarized parameters (P per cent, φ), the continuum at 5100 \AA and the broad $H\beta$, $H\alpha$ emission line fluxes and the $H\alpha$ polarized flux, using the equation given by O’Brien et al. (1998):

$$F_{\text{var}} = \sqrt{\sigma(F)^2 - e^2} / F_{\text{mean}},$$

where e^2 is the mean square value of the individual measurement uncertainty for N observations, i.e. $e^2 = \sum e(i)^2 / N$. There, N is the number of spectra, F denotes the mean flux over the whole observing period, $\sigma(F)$ is the standard deviation and $R(\text{max})/R(\text{min})$ is the ratio of the maximal to the minimal value of the measured parameters (or flux) in the monitored period. The parameter F_{var} is an inferred (uncertainty corrected) estimation of the variation amplitude with respect to the mean flux. In Table 3 (last three rows) the variability parameters for the continuum flux at 5100 \AA and the broad $H\alpha$ and $H\beta$ emission line flux are given from the paper of Shapovalova et al. (2010).

² The polarized continuum flux is obtained taking the continuum flux at 5100 \AA and polarization degree at 5500 \AA .

As it can be seen from Table 3, during the monitored period (2009–2014) the average fluxes and their amplitudes in broad lines and continuum were about two times bigger while F_{var} (variability) was two times smaller than in the period of spectral monitoring (1995–2007). The variability F_{var} for polarization parameters is not high (14 per cent for P , 7 per cent for φ). However, for the polarized $H\alpha$ line F_{var} is ~ 69 per cent that is considerably larger than the variability of another parameters. The polarization in $H\alpha$ is close to the zero level, that could be reason for the large variability. The maximum of the polarized $H\alpha$ flux ($F = (7.19 \pm 0.75) \times 10^{-14} \text{ erg cm}^{-2} \text{ s}^{-1}$; Table 2) was observed on 26.08.2011. At this time the broad $H\alpha$ and $H\beta$ emission line and polarized continuum at 5100 \AA were close to have the maximum fluxes, but the unpolarized (total) continuum flux was maximal in 01.05.2011–01.06.2011, i.e. 60–90 d before the maximum in the line flux (see Table 2 and Fig. 3). Obviously, we see a lag of response of the broad line to the continuum flux (see Fig. 3).

3.2 CCF analysis – dimension of the scattering regions

Using the reverberation method, which is the search for correlations between the broad emission line and continuum flux variations, it is possible to study geometry and dynamics of the BLR (see Peterson et al. 1993, and references therein). By analogy we used a long-term spectropolarimetric monitoring of 3C 390.3 to study the properties of the scattering gas geometry by reverberation method. To do this we applied the CCF analysis using first the interpolation method (so-called ICCF; see Gaskell & Sparke 1986). We interpolated the light curves in the unpolarized and polarized continuum (as well as in the $H\alpha$ and $H\beta$ lines), after that we used the CCF and computed the lags relative to the CCF peak.

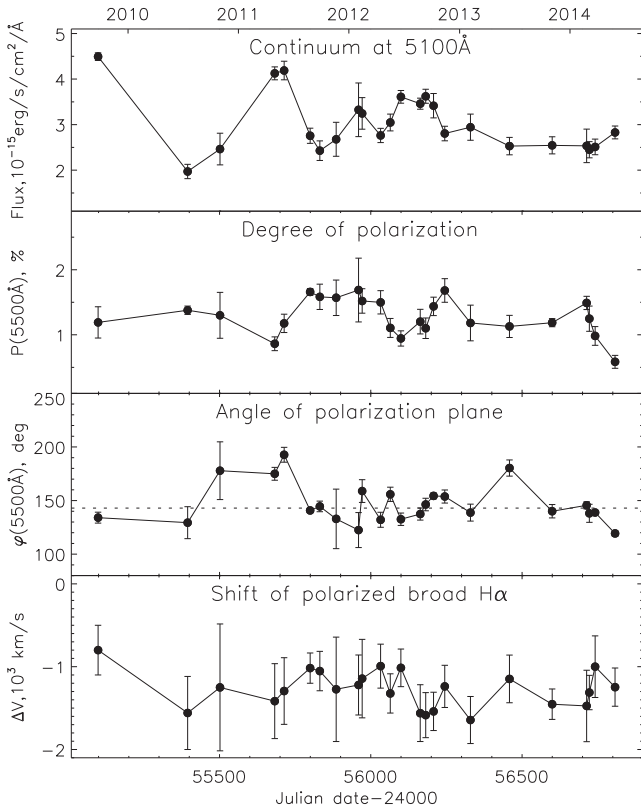


Figure 2. From top to bottom: the light curves of the total (unpolarized) continuum flux at 5100 Å in the rest frame, variation of the degree of the linear polarization P and angle of polarization plane of the continuum at 5500 Å in the rest frame and shift ΔV of the polarized broad $H\alpha$ line relatively to the systematic velocity.

In Fig. 4 (left) we plot the interpolated light curves of (from top to bottom) the polarized continuum, the broad $H\beta$, the broad $H\alpha$ and the polarized $H\alpha$ (thick lines) compared with the interpolated normalized light curves for the unpolarized continuum (thin line). As it can be seen in Fig. 4 (left) different lags between the unpolarized continuum (thin line) and mentioned fluxes are present.

Since different time series analyses can give different lags for the same set of data (see in more details Kovačević et al. 2014), therefore, we calculated the lags using z-transformed discrete correlation function (ZDCF; see Alexander 2013) and stochastic process estimation (SPE; Zu, Kochanek & Peterson 2011) in addition to the ICCF method. The estimated lags are given in Table 4.

We found that the lags between unpolarized and polarized continuum at 5100 Å are ~ 10 –40 d; between the unpolarized continuum and the broad $H\beta$ line ~ 60 –80 d; between the unpolarized continuum and broad $H\alpha$ flux ~ 140 –190 d; between the unpolarized continuum and polarized $H\alpha$ ~ 90 –160 d (see Table 4). In all three methods we obtained that the lag between the unpolarized and polarized continuum is significantly smaller than lags between the continuum and broad lines, that indicates that the variable polarized continuum is originating in a region which is significantly smaller than the BLR.

Note here that our lag estimates are in good agreements with these given in literature, as e.g. Shapovalova et al. (2010) obtained lags 127^{+18}_{-18} d for $H\alpha$ and 93^{+20}_{-18} d for $H\beta$.

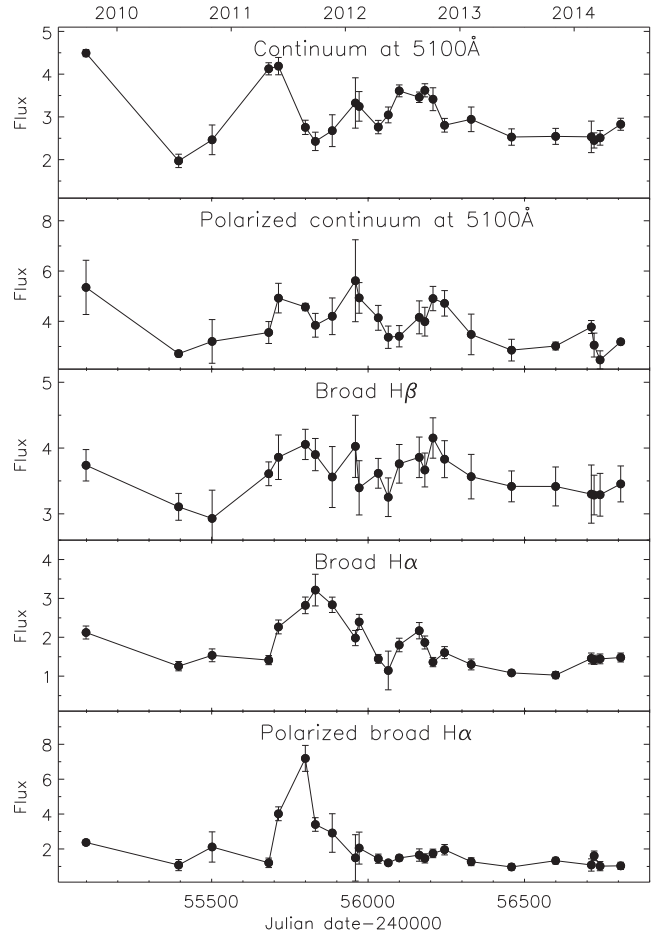


Figure 3. 3C 390.3 light curves – from top to bottom: the total and polarized continuum flux at 5100 Å in the rest frame; the broad $H\alpha$ and $H\beta$ and the polarized broad $H\alpha$ line. Flux units: continuum at 5100 Å in 10^{-15} erg cm $^{-2}$ s $^{-1}$ Å $^{-1}$; broad $H\beta$ in 10^{-13} erg cm $^{-2}$ s $^{-1}$; broad $H\alpha$ in 10^{-12} erg cm $^{-2}$ s $^{-1}$; polarized $H\alpha$ in 10^{-14} erg cm $^{-2}$ s $^{-1}$.

Table 3. Variability properties of the continuum end emission lines in spectra 3C 390.3.

Feature	$\langle F \rangle$	$\sigma(F)$	$\frac{R_{\text{(max)}}}{R_{\text{(min)}}}$	F_{var}	$\frac{F(H\alpha)}{F(H\beta)}$
$P(5500)$ (per cent)	2.01	0.28	1.58	0.14	
$\varphi(5500)$ ($^{\circ}$)	151.80	10.90	1.33	0.07	
$F(5100)$	3.02	0.63	2.28	0.21	
$F(\text{broad } H\beta)$	3.72	0.72	2.36	0.19	
$F(\text{broad } H\alpha)$	17.72	3.87	3.12	0.22	4.7
$F(\text{polarized } H\alpha)$	1.96	1.36	7.41	0.69	
$F(5100)$ 1995–2007	2.31	1.07	5.20	0.46	
$F(\text{broad } H\beta)$ 1995–2007	2.39	0.91	4.70	0.38	
$F(\text{broad } H\alpha)$ 1995–2007	9.42	3.36	3.40	0.35	3.94

Notes. Units: $F(5100)$ in 10^{-15} erg cm $^{-2}$ s $^{-1}$ Å $^{-1}$; $F(\text{polarized } H\alpha)$ in 10^{-14} erg cm $^{-2}$ s $^{-1}$ Å $^{-1}$; $F(\text{broad } H\beta)$ and $F(\text{broad } H\alpha)$ in 10^{-13} erg cm $^{-2}$ s $^{-1}$ Å $^{-1}$.

4 DISCUSSION

4.1 Polarized continuum

Using the results of our spectropolarimetric monitoring of 3C 390.3 (data for 24 epochs during 5 yr) we found the lag ~ 10 –40 d between the unpolarized and polarized continuum flux variations. The

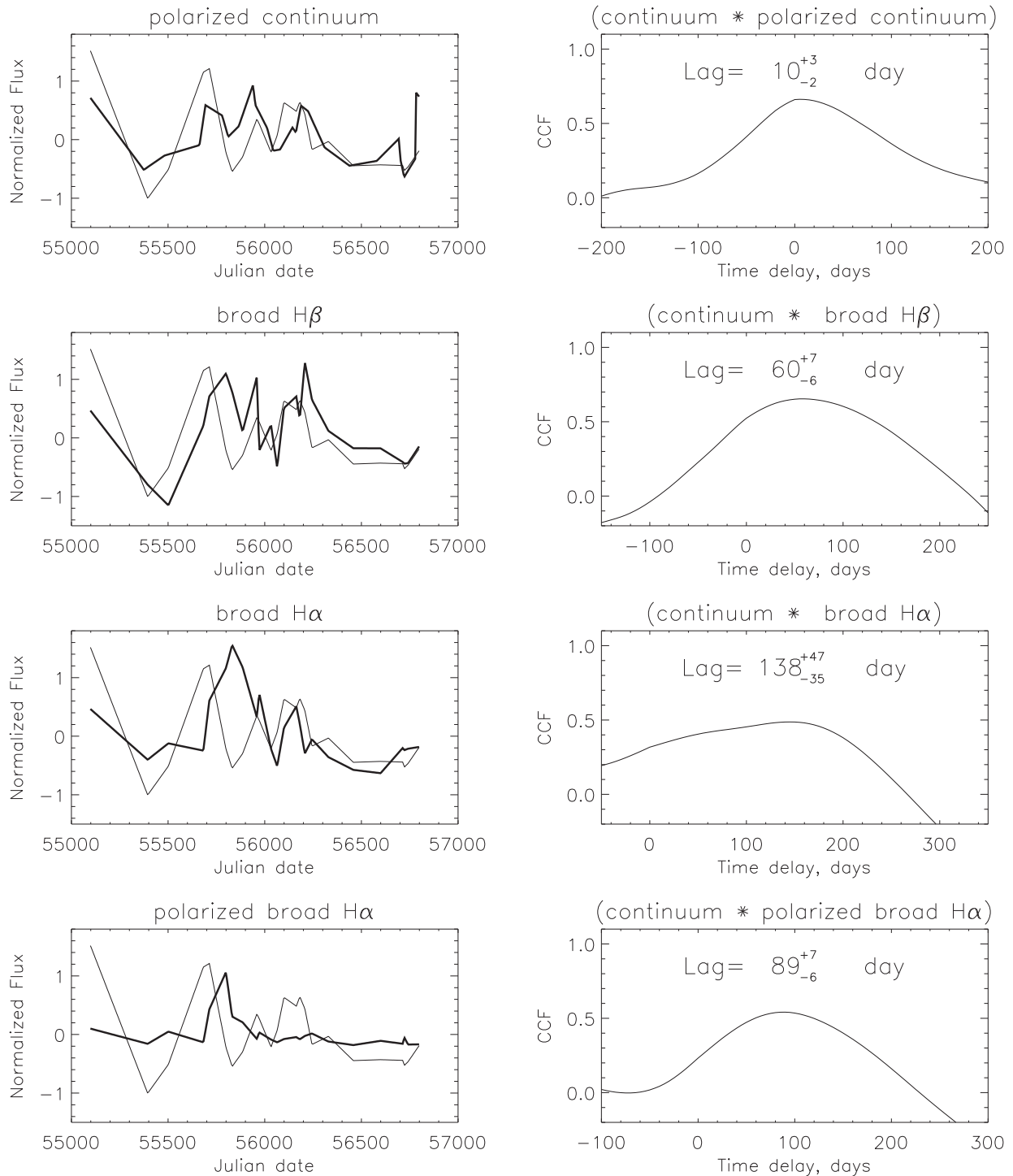


Figure 4. Left: the interpolated normalized light curves, from top to bottom (thick lines): the polarized continuum, the broad H β flux, the broad H α flux, the polarized H α flux compared with the unpolarized continuum (thin lines). Right: from top to bottom the lags between the unpolarized and polarized continuum at rest 5100 Å; the broad H β line, the broad H α line and the polarized H α fluxes.

estimated size of the BLR is significantly larger (lag ~ 60 –190 d). This indicates that the region of polarized radiation which contributes to the variability of the polarized continuum is more compact than the BLR in the case of 3C 390.3. A similar result (lag ~ 2 d) is obtained for Mrk 6 (Afanasiev et al. 2014a), where the BLR is estimated to be significantly larger than the scattering region. Gaskell et al. (2012) found that in the case of NGC 4151 the lag between the

unpolarized and polarized continuum flux variations is ~ 8 d and almost the same as the BLR lag, however, it seems that their error bars of the estimated lags are large (see their table 1 in Gaskell et al. 2012).

The average polarization angle ($\varphi = 152^\circ \pm 11^\circ$) of the continuum at rest wavelength 5500 Å is consistent and almost aligned with the radio jet angle $\sim 144^\circ$ (Leahy & Perley 1991). The variability of

Table 4. The lags obtained using different methods: ICCF – interpolation method (Gaskell & Sparke 1986); ZDCF – z-transformed discrete correlation function (Alexander 2013) and SPE – stochastic process estimation (Zu et al. 2011).

Lag between	ICCF	ZDCF	SPE
cnt – pol-cnt	10^{+3}_{-2}	27^{+9}_{-10}	39^{+7}_{-9}
cnt – broad H β	60^{+7}_{-8}	79^{+16}_{-15}	79^{+8}_{-9}
cnt – pol. broad H α	89^{+7}_{-9}	128^{+32}_{-29}	156^{+8}_{-21}
cnt – broad H α	138^{+47}_{-35}	184^{+28}_{-12}	186^{+7}_{-6}

φ is relatively small ($F_{\text{var}} \sim 7$ per cent, Table 3), but the degree of the linear polarization of the continuum changes as $F_{\text{var}} \sim 14$ per cent, that may indicate an additional continuum component to that in the nucleus. This is in favour of the results obtained by Arshakian et al. (2010). According to the results of very long baseline interferometry (VLBI) monitoring there are the observational evidence for the connection between the variable optical continuum nucleus of 3C 390.3 and the compact radio emission of the jet on the sub-parsec scale (Arshakian et al. 2010). To explain this correlation, Arshakian et al. (2010) suggested that the variable optical continuum emission is generated in the innermost part of the jet.

The polarization in the 3C 390.3 continuum probably has three sources: (i) we expect to have the polarization from the disc (light scattering in a plane-parallel disc atmosphere), with perpendicular polarization angle to the jet direction (and almost constant); (ii) scattering on the inner part of the torus, where the vector of polarization is aligned with the radio jet (without fast variability in the continuum polarization) and (iii) the synchrotron continuum emission of the jet (whose polarization vector is approximately perpendicular to the jet direction) that probably contributes to the variability in the continuum polarized light. This also can be seen in Fig. 5 where the variability in the continuum (open circles) has arc-like structure with respect to the jet direction (denoted with an arrow). The jet angle is taken from Alef et al. (1988, 1996).

The observed decrease of the polarization in the continuum as a function of wavelength may be caused by the Rayleigh scattering on the torus or the inverse Compton effect (Begelman & Sikora 1987) in the relativistic plasma jet. However, a detailed study of this effect requires modelling and it is out of the scope of this paper. Another possible explanation for decreasing polarization may be wavelength-dependent dilution by the host galaxy continuum, which will be redder than the AGN. However as we noted above the contribution of the host galaxy to the unpolarized flux is ~ 20 per cent, and the estimated contribution to the polarization is around 0.25 per cent. This cannot cause the observed changes in the optical polarization, which are about 1 per cent.

4.2 Polarized H α

There are several models proposed to explain the two-peak structure of the broad Balmer emission lines in 3C 390.3. A widely accepted model is the formation of the broad lines in a relativistic disc. However, there are some contradictions between these models and the polarization observations of 3C 390.3. Smith et al. (2004, 2005) proposed two mechanisms of polarization in the optical continuum and H α broad emission lines in Sy1 nuclei – equatorial (scattering on the inner part of the torus) and polar (scattering on the jet) polarization mechanisms. Both scattering components should be present in all broad line AGN, and their polarization properties can

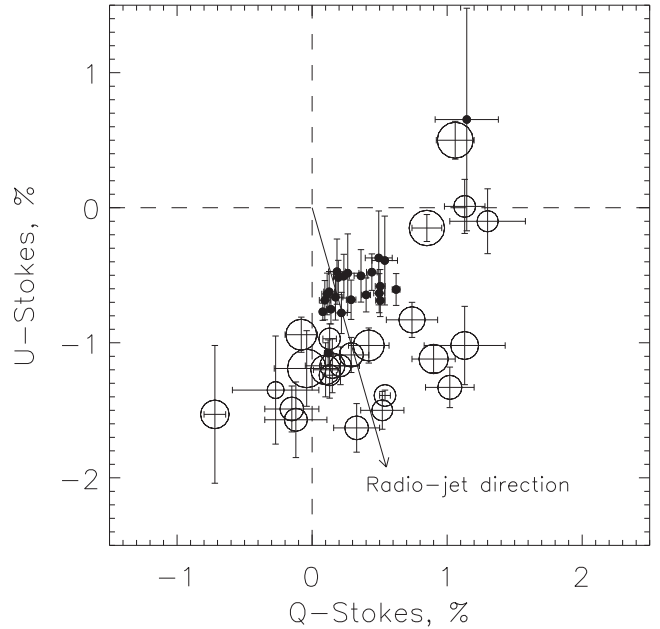


Figure 5. The variation of the continuum (open circles) in the Stokes parameters (U , Q) space with the projection of the radio jet direction (arrow). The dimension of circles corresponds to the intensity continuum flux at 5100 Å in the rest frame. The arrow represents the direction of the radio jet of 3C 390.3 in the U , Q space. The black full circles represent the H α broad line Stokes parameters measured in the frame of the broad line profile.

be broadly understood in terms of an orientation effect (unified model; see Antonucci, Hurt & Agol 1996). In the case of equatorial scattering model, the broad emission lines which are emitted from a rotating disc (or outer regions of accretion disc–BLR) have to show a double-peaked structure in the polarized light, similar as in the unpolarized light. The degree of polarization will be maximal in the broad line wings and a minimum is expected in the line centre. The angle φ of plane polarization is aligned with the projected disc rotation axis and hence with the radio source axis.

In the case of 3C 390.3, we observed an unexpected difference between the unpolarized and polarized broad line profile of H α : the unpolarized H α line profile has double-peaked structure with the blue peak at $V_r \sim -3500$ km s $^{-1}$ and red one at $V_r \sim +5000$ km s $^{-1}$. But the polarized H α line profile is single peaked and shifted to blue at $V_r \sim -1200$ km s $^{-1}$ with respect to the narrow component (or systematic velocity). Also, the degree of the linear polarization of H α is small (around 0.1–0.2 per cent, close to zero) and has a box-like shape without any significant structural details, i.e. it seems that the broad H α line is almost completely depolarized. This is contrary to the equatorial scatter model. On the other hand in 3C 390.3 polarization angle (φ) is parallel to the pc-jet axis as it is expected in the equatorial scatter model (see Fig. 5 – full circles).

It should be noted that Corbett et al. (2000) considered a model of 3C 390.3 in which H α photons emitted by a biconical flow are scattered by the inner wall of the torus. Thus, the scattering plane is perpendicular to the radio jet (e.g. E vector parallel to pc-jet axis) and produces a single-peaked scattered H α line profile. However, this model does not agree with the optical monitoring data for the BLR, where the double-peaked broad emission line is formed. The CCF analysis for the H β and H α line wings in 3C 390 shows that there is no a significant delay in the variation of the line wings with respect to the central part of the line, or relative to each other. The flux in the H β line wings and core also varied simultaneously. This

result indicates a dominant circular motion in the BLR and it is in favour of a model in which the main contribution to the broad line fluxes originates in the accretion disc and not from the biconical flow (Dietrich et al. 1998, 2012; Shapovalova et al. 2010; Popović et al. 2011; Zheng 2011, 2013).

4.2.1 Polarized profile of the broad H α line

In Fig. 6 we present the main unpolarized (first panel) and polarized (second panel) broad H α shapes. The polarized and unpolarized lines are normalized on their intensities in order to compare the profile variability. As it can be seen in Fig. 6 there is no big change in the polarized and unpolarized line profile. The unpolarized H α line has a double-peaked profile, the peaks are located (within the error bars) as earlier measured (see e.g. Popović et al. 2011): the blue peak is located at $V_b \sim -3500 \text{ km s}^{-1}$ while the red peak had $V_r \sim 5000 \text{ km s}^{-1}$ for H α . Contrary, the polarized H α is single peaked and shifted to the blue for about -1200 km s^{-1} .

Also, in the third panel of Fig. 6 we present the Stokes U parameter. It is interesting that the U parameter has a box-like shape that indicates presence of a depolarization region, i.e. presence of the warm gas between an observer and accretion disc.

The Stokes parameters for the broad line are present in Fig. 5 as black full circles. It is interesting that they are following the jet direction. It means that there is a slight polarization from the disc,

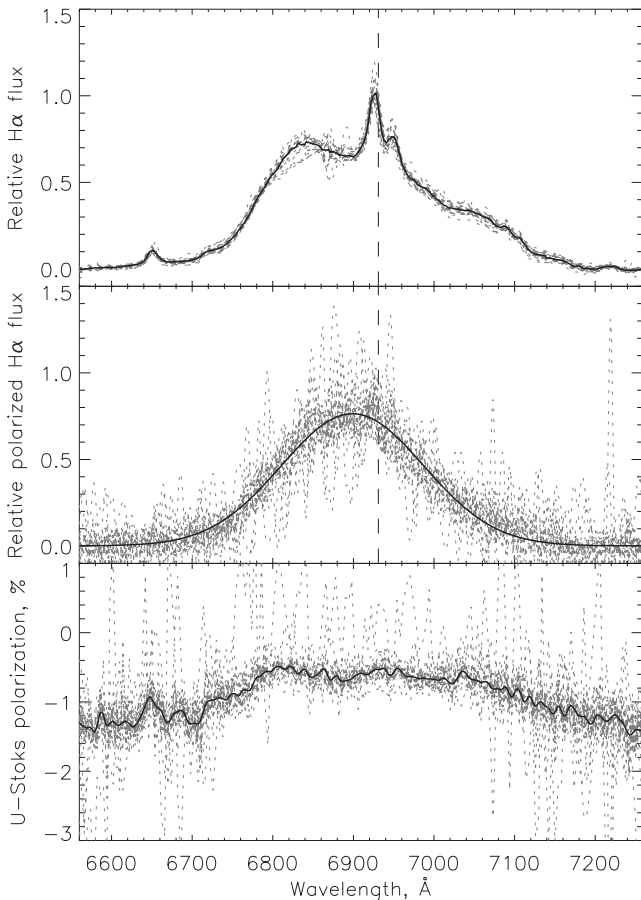


Figure 6. From top to bottom: the broad H α line, polarized H α and polarization parameter U . Faint dashed lines represent observations from different epochs and solid bold lines represent averaged profiles of the unpolarized and polarized H α and parameter U .

but in contrast to Mrk 6 (see Afanasiev et al. 2014a), the effect of the equatorial scattering cannot be seen.

4.3 Polarization – connection between disc and jet

To speculate about the possible model that can explain the unpolarized and polarized H α line profile and the continuum, let us recall several observational facts.

(i) 3C 390.3 is a powerful radio source with two lobes, Fanaroff and Riley Class II (FR II) radio galaxy with relatively strong compact core. There are two extended lobes in position angle PA $\sim 144^\circ$, separated by $\sim 223 \text{ arcsec}$ each with a hotspot at the end (Leahy & Perley 1991). Also, there is a weak well collimated thin jet in PA $\approx -37^\circ$, linking the core with the northern lobe (Leahy & Perley 1995). In this parsec-jet the VLBI observations at 5 GHz detected superluminal motion (with $v/c \sim 4$; Alef et al. 1988, 1996).

(ii) It seems that a part of the optical continuum is coming from the jet since the optical continuum and radio emission from a jet structure are correlated (Arshakian et al. 2008, 2010).

(iii) The unpolarized H α shape and its variability are in agreement with the disc emission model (Shapovalova et al. 2010; Popović et al. 2011). However, there is a central component shifted to the red from 300 to 800 km s^{-1} and additionally the broad double-peaked H α line shows a blue shift, indicating a wind at the disc surface with velocities from -300 to -800 km s^{-1} (Popović et al. 2011). Contrary, the polarized H α broad line profile is single peaked with the blue shift of 1200 km s^{-1} , that is not in the favour of the disc model (Smith et al. 2004, 2005), but seems to agree with two-side outflow model (Corbett et al. 1998, 2000).

To explain all these observational facts, one can take into account a complex BLR model (see Fig. 7), where the disc-like BLR is covered by an outflowing region (the wind with speed around -1200 km s^{-1}) – with a number of warm clouds which also can emit the H α line. This region can depolarize the disc-like emission. The two-component BLR (disc covered by an outflowing

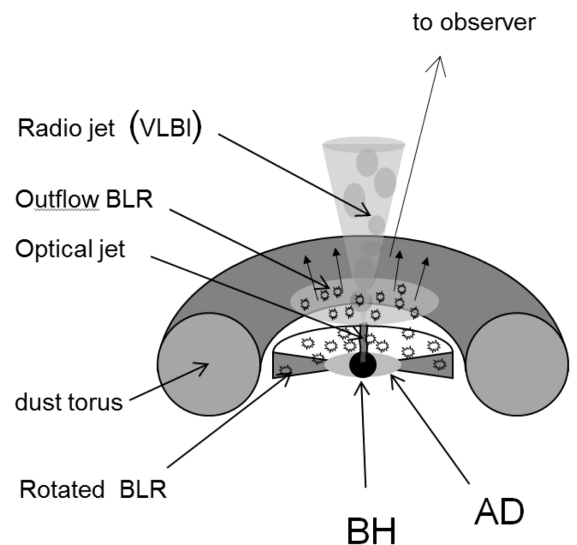


Figure 7. Sketch illustrating a possible central region of 3C 390.3. Two-component BLR: the double-peaked lines originate in the disc-like region, and depolarization is by warm clouds in an outflowing part of the BLR. The part of the variable polarized continuum seems to be emitted from the jet.

region of randomly distributed clouds) seems to be a good approximation for nearby AGN (Kollatschny & Zetzl 2013), as well as for a number of single-peaked AGN (see in more details Bon et al. 2009).

One can expect that the outflowing region with warm gas can contribute to the additional electron scattering, which may actually cause the line emission to be polarized. However, in the outflowing region, the polarization vector is parallel to the disc plane, and practically depolarizes the polarized light from equatorial scattering.

In a scenario of the two-component model (disc+outflowing components; Popović et al. 2011), the blueshifted $H\alpha$ component is coming from the outflowing part of the BLR, and cannot be (self)depolarized, while the disc-like component is depolarized by this region.

Moreover, the two-component BLR model is able to explain both, the double-peaked unpolarized emission and depolarization of the broad $H\alpha$ line (box-like structure in the polarized line profile, see Fig. 1). Alternatively, the hot depolarization gas may have an inflowing component that is in contradiction with results obtained in the long-term profile line analysis (see Popović et al. 2011).

The part of the continuum is originating in this jet-like part (outflow) and it may be the reason for the wavelength-dependent polarization in the continuum, and relatively high level of the continuum polarization (around 2 per cent, in comparison with Sy1 that is around 1 per cent; see Afanasiev et al. 2014a).

5 CONCLUSION

We presented results of the spectropolarimetric monitoring of 3C 390.3, obtained at 24 epochs in the period of 2009–2014. The galaxy has been observed with 6-m telescope of SAO observatory using SCORPIO-2 instrument with spectral resolution of 7–10 Å in the spectral range between 4000 and 8000 Å. Also, we observed and estimated the contribution of the ISM polarization to the observed 3C 390.3 polarization. We measured polarization parameters for the continuum at 5100 Å (rest wavelength) and $H\alpha$ line and their variabilities, and explored the lag between the unpolarized and polarized flux. On the basis of our investigation we can outline the following conclusions.

(i) During the 5-yr monitoring period we found variation in the broad line and continuum polarization parameters. We found a lag of 10–40 d between the polarized and unpolarized continuum flux variation at 5100 Å. This lag is significantly smaller than one we found for the BLR (lag for $H\beta$ is 60–80 d and for $H\alpha$ is 140–190 d), i.e. the scattering region of the continuum probably is not the BLR (accretion disc). It seems that the polarized continuum has a component which is coming from the disc (E vector is orientated in the jet direction), and another, that contributes to variability that may be synchrotron contribution to the continuum from a pc-jet component.

(ii) The unpolarized double-peaked broad emission $H\beta$ and $H\alpha$ lines are observed as single-peaked polarized lines. The polarized line is shifted to the blue for about -1200 km s^{-1} , and such profile was not expected in the case of the equatorial scattering. Additionally, we observed a box-like profile of the line polarization (that has a small value ~ 0.1 per cent) that indicates depolarization by the warm gas. Taking into account the results from the modelling of variability, we proposed that depolarization region is an outflowing region located above the disc-like emission region (that emits double-peaked lines) and plays a role in the disc line depolarization.

ACKNOWLEDGEMENTS

The results of observations were obtained with the 6-m BTA telescope of the Special Astrophysical Observatory of the Russian Academy of Sciences, operating with the financial support of the Ministry of Education and Science of Russian Federation (state contracts no. 16.552.11.7028, 16.518.11.7073). The authors also express appreciation to the Large Telescope Program Committee of the RAS for the possibility of implementing the program of Spectropolarimetric observations at the BTA. This work was supported by the Russian Foundation for Basic Research (project N12-02-00857) and the Ministry of Education, Science and Technological Development (Republic of Serbia) through the project Astrophysical Spectroscopy of Extragalactic Objects (176001). We thank to M. Gabdееv for help in spectropolarimetric observations. LČP thanks to the COST Action MP1104 ‘Polarization as a tool to study the Solar system and beyond’ for support. We thank to an anonymous referee for very useful comments.

REFERENCES

- Afanasiev V. L., Amirkhanyan V. R., 2012, *Astrophys. Bull.*, 67, 438
 Afanasiev V. L., Moiseev A. V., 2005, *Astron. Lett.*, 31, 194
 Afanasiev V. L., Moiseev A. V., 2011, *Balt. Astron.*, 20, 363
 Afanasiev V. L., Popović L. Č., Shapovalova A. I., Borisov N. V., Ilić D., 2014a, *MNRAS*, 440, 519
 Afanasiev V. L., Rosenbush V. K., Kiselev N. N., 2014b, *Astrophys. Bull.*, 69, 211
 Alef W., Gotz M. M. A., Preuss E., Kellermann K. I., 1988, *A&A*, 192, 53
 Alef W., Gotz M. M. A., Preuss E., Kellermann K. I., Qiu Y. H., 1996, *A&A*, 308, 376
 Alexander T., 2013, preprint ([arXiv:1302.1508](https://arxiv.org/abs/1302.1508))
 Antonucci R., Hurt T., Agol E., 1996, *ApJ*, 456, L25
 Arshakian T. G., León-Tavares J., Lobanov A. P., Chavushyan V. H., Popović L., Shapovalova A. I., Burenkov A., Zensus J. A., 2008, *Mem. Soc. Astron. Ital.*, 79, 1022
 Arshakian T. G., León-Tavares J., Lobanov A. P., Chavushyan V. H., Shapovalova A. I., Burenkov A. N., Zensus J. A., 2010, *MNRAS*, 401, 1231
 Barr P. et al., 1980, *MNRAS*, 193, 562
 Barr P., Willis A. J., Wilson R., 1983, *MNRAS*, 202, 453
 Begelman M. C., Sikora M., 1987, *ApJ*, 322, 650
 Bon E., Popović L. Č., Gavrilović N., La Mura G., Mediavilla E., 2009, *MNRAS*, 400, 924
 Chakrabarti S. K., Wiita P., 1994, *ApJ*, 434, 518
 Clavel J. C., Wamsteker W., 1987, *ApJ*, 320, L9
 Corbett E. A., Robinson A., Axon D. J., Young S., Hough J. H., 1998, *MNRAS*, 296, 721
 Corbett E. A., Robinson A., Axon D. J., Young S., 2000, *MNRAS*, 319, 685
 Dietrich M. et al., 1998, *ApJS*, 115, 185
 Dietrich M. et al., 2012, *ApJ*, 757, 53
 Eracleous M., Livio M., Halpern J. P., Storchi-Bergmann T., 1995, *ApJ*, 438, 610
 Eracleous M., Halpern J. P., Livio M., 1996, *ApJ*, 459, 89
 Gaskell C. M., 1983, in *Proc. 24th Liege Int. Astrophys. Colloq., Quasars and Gravitational Lenses*. Univ. Liege, Cointe-Ougree, p. 471
 Gaskell C. M., 1996, *ApJ*, 464, L107
 Gaskell C. M., Sparke L. S., 1986, *ApJ*, 305, 175
 Gaskell C. M., Goosmann R. W., Merkulova N. I., Shakhovskoy N. M., Shoji M., 2012, *ApJ*, 749, 148
 Gliozzi M., Sambruna R. M., Eracleous M., 2003, *ApJ*, 584, 176
 Gupta A. C., Srivastava A. K., Wiita P. J., 2009, *ApJ*, 690, 216
 Heiles C., 2000, *AJ*, 119, 923
 Hsu J.-C., Breger M., 1982, *ApJ*, 262, 732
 Inda M. et al., 1994, *ApJ*, 420, 143
 Jovanović P., Popović L. Č., Stalevski M., Shapovalova A. I., 2010, *ApJ*, 718, 168

- Kishimoto M., Antonucci R., Boisson C., Blaes O., 2004, *MNRAS*, 354, 1065
- Kollatschny W., Zetzl M., 2013, *A&A*, 558, A26
- Kovačević A., Popović L. Č., Shapovalova A. I., Ilić D., Burenkov A. N., Chavushyan V. H., 2014, *Adv. Space Res.*, 54, 1414
- Leahy J. P., Perley R. A., 1991, *AJ*, 102, 537
- Leahy J. P., Perley R. A., 1995, *MNRAS*, 277, 1097
- Leighly K. M., O'Brien P. T., 1997, *ApJ*, 481, L15
- Netzer H., 1982, *MNRAS*, 198, 589
- O'Brien P. T. et al., 1998, *ApJ*, 509, 163
- Penston M. V., Perez E., 1984, *MNRAS*, 211, 13
- Perez E., Mediavilla E., Penston M. V., Tadhunter C., Moles M., 1988, *MNRAS*, 230, 353
- Peterson B. M., Ali B., Horne K., Bertram R., Lane N. J., Pogge R. W., Wagner R. M., 1993, *ApJ*, 402, 469
- Popović L. Č., 2012, *New Astron. Rev.*, 56, 74
- Popović L. Č. et al., 2011, *A&A*, 528, A130
- Rokaki E., Boisson C., Collin-Souffrin S., 1992, *A&A*, 253, 57
- Schmidt G. D., Elston R., Lupie O. L., 1992, *AJ*, 104, 1563
- Sergeev S. G., Pronik V. I., Peterson B. M., Sergeeva E. A., Zheng W., 2002, *ApJ*, 576, 660
- Serkowski K., Mthewson D. S., Ford V. L., 1975, *ApJ*, 196, 261
- Shapovalova A. I. et al., 2001, *A&A*, 376, 775
- Shapovalova A. I. et al., 2010, *A&A*, 517, A42
- Smith J. E., Robinson A., Alexander D. M., Young S., Axon D. J., Corbett E. A., 2004, *MNRAS*, 350, 140
- Smith J. E., Robinson A., Young S., Axon D. J., Corbett E. A., 2005, *MNRAS*, 359, 846
- Tao J., Fan J., Qian B., Liu Y., 2008, *AJ*, 135, 737
- Veilleux S., Zheng W., 1991, *ApJ*, 377, 89
- Wamsteker W., Wang T.-G., Schartel N., Vio R., 1997, *MNRAS*, 288, 225
- Wozniak P. R., Zdziarski A. A., Smith D., Madejski G. M., Johnson W. N., 1998, *MNRAS*, 299, 449
- Yee H. K., Oke J. B., 1981, *ApJ*, 248, 472
- Zhang X.-G., 2011, *MNRAS*, 416, 2857
- Zhang X.-G., 2013, *MNRAS*, 431, L112
- Zheng W., 1996, *AJ*, 111, 1498
- Zheng W., Veilleux S., Grandi S. A., 1991, *ApJ*, 381, 121
- Zu Y., Kochanek C. S., Peterson B. M., 2011, *ApJ*, 735, 1

This paper has been typeset from a $\text{\TeX}/\text{\LaTeX}$ file prepared by the author.